ACTA IMEKO
ISSN: 2221-870X
June 2026, Volume 15, Number 2, 1 - 6

Spatiotemporal correlation using inverse triangulation technique with a variable pseudorandom pattern projector for 3D stereo measurement

Daniel J. Regner[1], Moacir Wendhausen[1], Bianca M. Rosa[1], Luan C. Corrêa[1], João Facco[1], Tiago C. Pinto[1], Armando Albertazzi[1]

[1] *Labmetro – Mechanical Enginnering Department, Federal University of Santa Catarina, Florianópolis, Brazil*

ABSTRACT
In this paper, we propose an innovative 3D reconstruction approach based on stereo vision that combines inverse triangulation with spatiotemporal correlation algorithms. The inverse triangulation technique allows the correspondence search to be performed in an ordered manner within object space. In this way, the proposed approach performs the correspondence search using well-defined three-dimensional regions in object space. These regions are structured as regular grids centered on each analyzed point (X, Y, Z) within the measurement volume. The spatiotemporal correlation across the projected regions determines the optimal Z value, resulting in a structured and reliable 3D reconstruction. This proposed approach is intended for future applications focused on the underwater inspection of offshore structures in the oil and gas industry.

Section: RESEARCH PAPER

Keywords: inverse triangulation; 3D reconstruction; spatiotemporal correlation; active stereo; random pattern laser projection

Citation: D. J. Regner, M. Wendhausen, B. M. Rosa, L. C. Corrêa, João Facco, T. C. Pinto, A. Albertazzi, Spatiotemporal correlation using inverse triangulation technique with a variable pseudorandom pattern projector for 3D stereo measurement, Acta IMEKO, vol. 15 (2026) no. 2, pp. 1-6. DOI: 10.21014/actaimeko.v15i2.2258

Section Editor: Maik Rosenberger, Ilmenau University of Technology, Germany

Received November 30, 2025; **In final form** May 11, 2026; **Published** June 2026

Funding: FINEP - Brazilian Funding Authority for Studies and Projects, Brazil.

Corresponding author: Daniel Regner, e-mail: daniel.regner@labmetro.ufsc.br

1. INTRODUCTION

To support the reconstruction process, active stereo vision techniques typically rely on the projection of structured light patterns [1]. These techniques aim to enrich the scene with additional texture for point correspondence between images, enabling measurements on low-texture surfaces or under unfavourable lighting conditions. Among such techniques, fringe projection combined with phase-shifting algorithms can be highlighted [2], as well as color-coded fringe patterns [3], in which the structured-light stereo approach is proposed to recover dynamic shapes with reduced occlusion and extended viewing range. Another strategy involves the projection of random patterns generated from coherent light, such as laser illumination forming a granular random pattern of bright and dark regions, known as speckle, as demonstrated in [4] and [5], which validate the robustness of single-shot 3D measurement techniques in dynamic scene analysis. In [6], a comparison between variable laser speckle projection and LED array projection using temporal correlation on the accuracy of 3D reconstruction is investigated. As shown in [7], the influence of different speckle projection patterns on the accuracy of 3D reconstruction in underwater conditions was investigated. In [8], a pseudorandom-grid structured-light pattern is projected using a DOE, and 3D reconstruction is achieved by triangulating grid-points identified by a CNN. To the best of our knowledge, no previous work uses the inverse triangulation with spatiotemporal correlation.

Unlike conventional stereo matching, which relies on matching image-space windows [9], the approach proposed in this paper performs correspondence search using three-dimensional regions (3D patches) defined in object space. The proposed innovation uses inverse triangulation [10] and spatiotemporal correlation with a custom-developed variable pseudorandom pattern projection. This approach enables an object-space organization of the point cloud with the range and resolution defined by the user. This algorithm was successfully

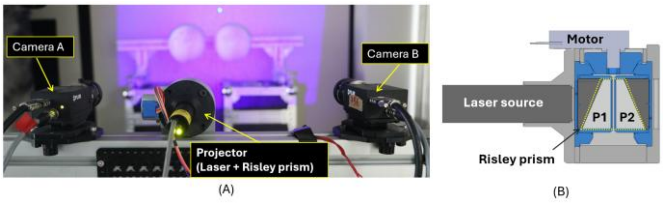

Figure 1. Vision system used: (A) two cameras, a pseudorandom pattern laser, (B) laser and Risley prism couplet to a motor.

applied in fringe projection and temporal correlation [10], [11], but in this work is applied for the first time in spatiotemporal correlation using a variable pseudorandom pattern projector.

2. METHODS AND PROCEDURES

The experimental validation was conducted using a custom-built active stereo vision system designed for high-resolution 3D measurement. The image acquisition system consists of a pair of FLIR cameras, labelled as Camera A and Camera B in Figure 1 (A), with 2048 × 2048 pixel resolution (4 MP), equipped with Schneider Xenon Topaz 2.0/25 mm lenses and band-pass filters at (465 ± 70) nm. The stereo vision setup has a baseline of 320 mm and a working distance of 1.5 m.

The structured light projector uses a blue laser with a wavelength of 450 nm and 100 mW, and a Diffractive Optical Element (DOE) to project a 30° × 30° divergent 40,000 dots pseudorandom matrix. The laser and the DOE are integrated with a Risley prism [12], composed of a motor and a pair of counter-rotating wedge prisms P1 and P2, as shown in Figure 1 (B), to control the vertical displacement of the projected pattern in object space. Image acquisition is hardware-synchronized with the angular displacement of the Risley prism, as illustrated in Figure 1 (B).

Figure 2 illustrates the image acquisition of a pseudorandom pattern projected onto a pair of spheres.

The adopted 3D reconstruction principle is inverse triangulation. Unlike conventional matching algorithms that scan windows in image space based on epipolar geometry [13], this method performs the correspondence search by scanning three-dimensional regions (3D patches) defined in the object space within a pre-defined measurement volume.

As proposed in [10], the inverse triangulation method consists of fixing two spatial coordinates (X, Y) of a 3D point and numerically searching for the coordinate Z that best satisfies a matching condition. Under this criterion, a scan is defined along Z within the pre-established measurement volume, projecting each 3D point onto the left and right image planes, as shown in Figure 3. The criterion adopted for point matching is defined according to the established principle, which may be: phase

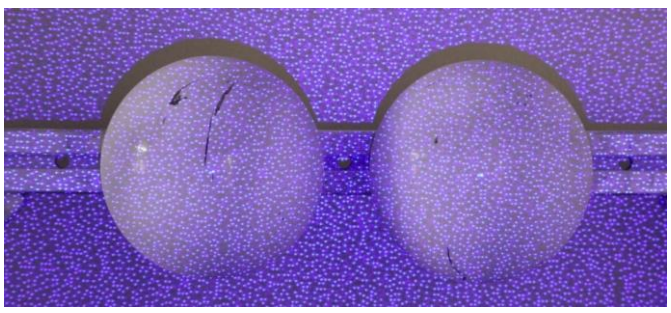

Figure 2. The pseudorandom pattern projected onto two spherical surfaces.

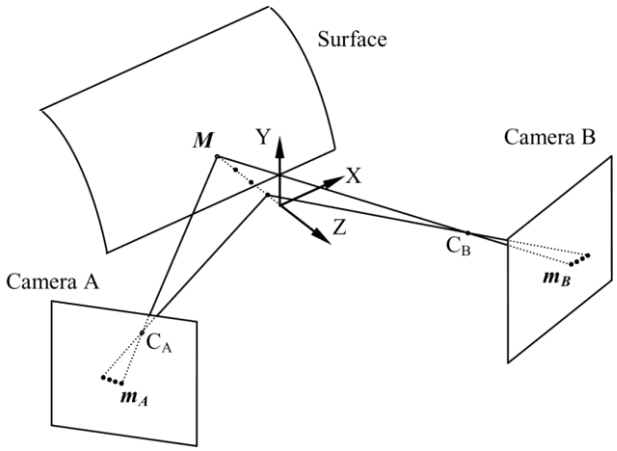

Figure 3. Inverse triangulation principle, adapted from [10].

difference, spatial correlation, temporal correlation, or spatiotemporal correlation.

The coordinate Z corresponding to the point on the object's surface, M in Figure 3, is the one that maximizes the correspondence between the projections. This process allows for the generation of a regular point cloud, characterizing a grid (X, Y) with spacing previously defined by the user. The approach is compatible with different structured light techniques and can achieve sub-pixel matching accuracy.

In this work, the inverse triangulation method employs the spatiotemporal criterion for point matching, and the 3D reconstruction process begins with the definition of a regular 3D point grid on object space, with a defined step size along the X, Y, and Z directions. For each Z in the correspondence search process, a 3D rectangular patch composed with the coordinate of interest at center and its $N \times N$ neighbors are mathematically projected in both images. The intensities of the correspondent subpixel positions of the projected points are interpolated over T images, resulting in intensity vectors of length $N \times N \times T$, used to compute the correlation value via Zero-mean Normalized Cross-Correlation (ZNCC) [13] described in equation (1):

$$\rho(i,j,i',j') = \frac{\sum_{t=1}^{N}[g(i,j,t) - \mathrm{g}][g'(i',j',t) - \bar{g}']}{\sqrt{\sum_{t=1}^{N}[g(i,j,t) - \bar{g}]^2}\,\sqrt{\sum_{t=1}^{N}[g'(i',j',t) - \bar{g}']^2}}, \quad (1)$$

where $g(i,j,t)$ and $g'(i',j',t)$ represents the vector pixel intensity along t the image and $\overline{g}$ and $\overline{g}'$ the mean value, respectively.

This process is repeated for each X, Y, Z in the measurement volume, and for each X, Y the best correlation along Z values define the Z coordinate. The use of spatiotemporal correlation aims to reduce the number of required images, while also minimizing the size of the 3D patch in object space, ensuring that the resulting vector is still sufficiently large for accurate correlation. A diagram of the inverse triangulation for the Spatiotemporal Correlation can be seen in Figure 4.

The evaluation methodology uses acquisitions of different calibrated geometries: a planar surface, spheres, and a pipe-like part, illustrated in Figure 5.

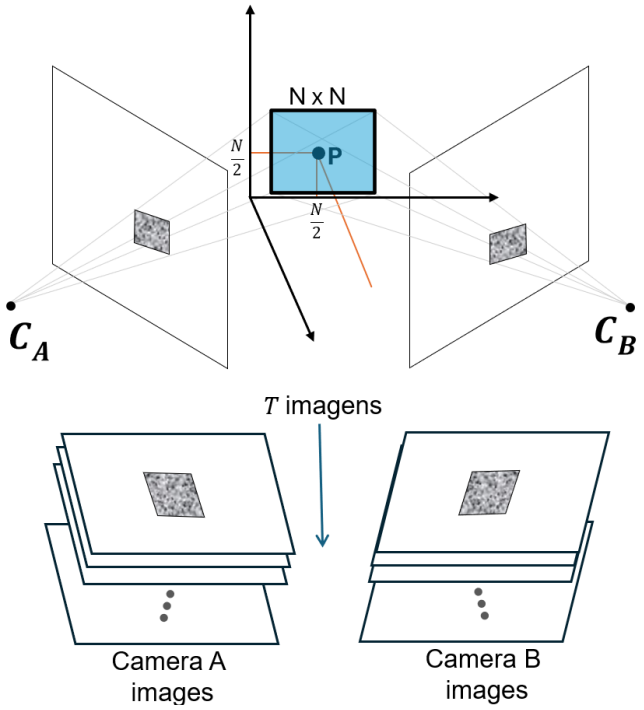

Figure 4. From a $N \times N$ 3D patch centred on P, reproject onto image planes correlate the patch along T images to identify the best Z value.

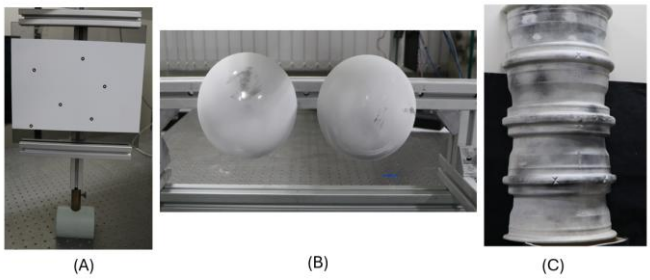

Figure 5. A plane (A), two spheres (B), and a pipe-like part (C) calibrated to be used as reference.

3. RESULTS

The experimental validation of the proposed system is presented in two main stages: parameter optimization and metrological performance assessment. The primary objective was to demonstrate that the spatiotemporal correlation approach could achieve a measurement accuracy comparable to traditional temporal methods while significantly reducing the data acquisition volume.

3.1. Patch optimization

To balance measurement accuracy with acquisition time, an optimization study was conducted. First, the variability of the pattern was analysed to determine the minimum motor displacement required between images, by analysing the mean absolute deviation (MAD) of regions across image sequences. 10 motor steps showed the highest pattern variability while minimizing the total required displacement, corresponding to a 5° rotation of the prisms.

Once the minimum number of steps was defined, all subsequent acquisitions were performed using this value and a 1 mm step size in the 3D grid. Acquisitions with many images

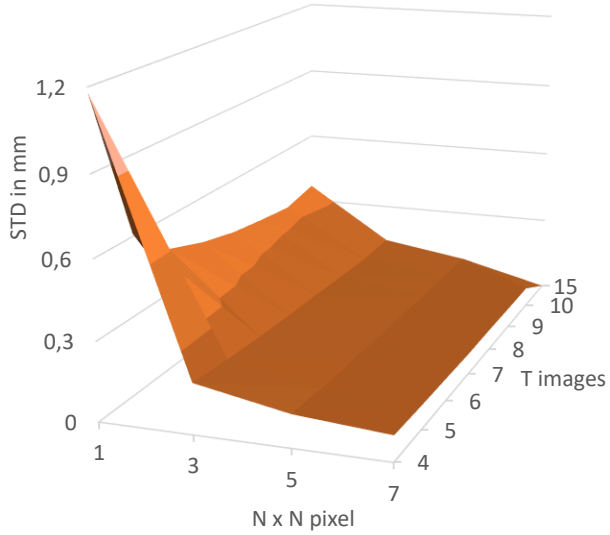

Figure 6. Standard deviation analysis over $N \times N$ kernel and T images combination to identify the optimal patch size.

(i.e., 15) were used to determine the optimal size of the 3D patch ($N \times N$) and the number T of temporal images, aiming to balance the reduction of $N \times N \times T$ with the quality of the plane measurement. As shown in Figure 6, different combinations of spatial and temporal windows were tested to minimize the standard deviation.

The standard deviation (0.17 mm) of distances between a fitted plane and the measured points determines the optimal patch size ($N \times N \times T$) as ($3 \times 3 \times 5$).

The measurements of the plane, spheres, and the pipe were performed using the determined values to access the resulting measurement uncertainty, and compared with pure temporal technique with a patch size of ($1 \times 1 \times 15$).

3.2. Flatness error

The assessment of flatness error served as the primary metric for evaluating the noise reduction capabilities and reconstruction accuracy of the proposed algorithm. As depicted in Figure 7, the flatness error, defined as the peak-valley deviation of reconstructed points from a mathematically fitted reference plane, was quantified at three distances: 1000 mm, 1250 mm, and 1500 mm. The quantitative data reveals that the spatiotemporal approach consistently outperformed the purely temporal method across all tested ranges. At the closest distance of 1000 mm, the temporal method exhibited a flatness error of 2.26 mm, whereas the spatiotemporal method significantly reduced this value to

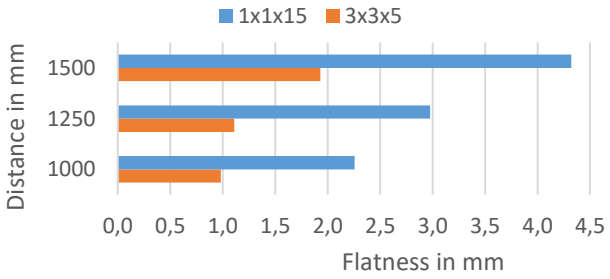

Figure 7. Flatness error for temporal (blue) and spatiotemporal correlation (orange).

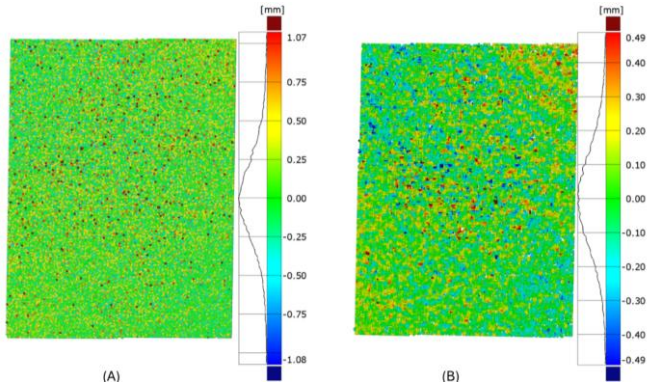

Figure 8. Fitting plane of (A) temporal and (B) spatiotemporal correlation reconstruction.

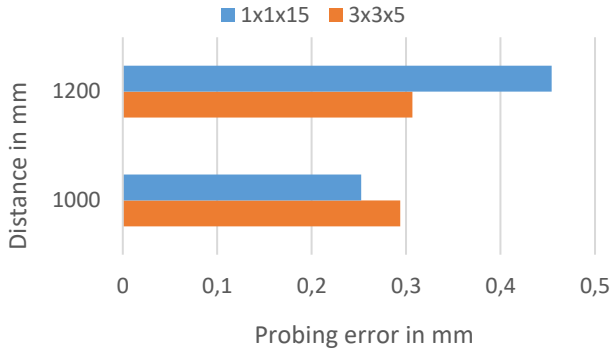

Figure 10. Probing error of fitted sphere reconstruction from temporal (blue) and spatiotemporal (orange) technique.

0.98 mm. This trend of superior performance persisted at the maximum range of 1500 mm, where the temporal method's error escalated to 4.32 mm, while the spatiotemporal method maintained a considerably lower error of 1.93 mm, effectively halving the reconstruction error.

These quantitative improvements are visually corroborated by the surface reconstruction maps presented in Figure 8. The reconstruction generated using the temporal method displays a noticeably grainy texture characterized by high-frequency noise, indicating that it was insufficient to fully filter out noise when relying solely on a single point temporal history. In contrast, spatiotemporal reconstruction appears significantly smoother and more coherent. This improvement is attributed to the spatial interpolation across the patch, which functions as an intrinsic local smoothing filter during the correlation process, and a bigger correlation vector, resulting in a more uniform surface with fewer outliers despite the substantial reduction in the number of acquired images.

3.3. Form and scale error

Subsequent to the planar surface evaluation, the volumetric performance of the measurement system was assessed using calibrated spheres to quantify both probing error and scale error. A comparative analysis was conducted between the baseline temporal and spatiotemporal algorithms at standoff distances of 1000 mm and 1200 mm.

Qualitatively, the reconstruction integrity is visualized in Figure 9, which presents the point clouds of the fitted spheres for both techniques. The residual distribution for 3 σ, represented by the colour maps, indicates that the spatiotemporal reconstruction achieves a surface density and coherence comparable to the temporal baseline, despite the substantial reduction in input data. This reinforces the quantitative evidence that spatiotemporal correlation effectively balances local surface definition with global geometric fidelity, establishing it as a highly efficient alternative for 3D metrological applications.

As illustrated in Figure 10, the probing error exhibits a distinct dependency on the standoff distance. At the proximal range of 1000 mm, the temporal method yielded a marginally superior probing error of approximately 0.25 mm, compared to 0.29 mm for the spatiotemporal method. However, at the extended range of 1200 mm, the spatiotemporal approach demonstrated enhanced robustness, maintaining a probing error of approximately 0.30 mm. In contrast, the temporal method experienced a significant degradation in performance, with the error increasing to approximately 0.45 mm. These findings suggest that the spatial constraints imposed by the 3 × 3 kernel effectively mitigate the signal-to-noise ratio degradation typically associated with increased measurement distances in active stereo systems.

Regarding dimensional integrity, Figure 11 depicts the scale error, derived from the normalized Euclidean distances between the fitted sphere centres. Both methodologies exhibited high dimensional fidelity, maintaining scale errors consistently below 0.15 % across the evaluated working volume. At 1000 mm, the spatiotemporal method presented a slight advantage, exhibiting an error of approximately 0.125 % versus 0.13 % for the temporal method. At 1200 mm, the performance of both

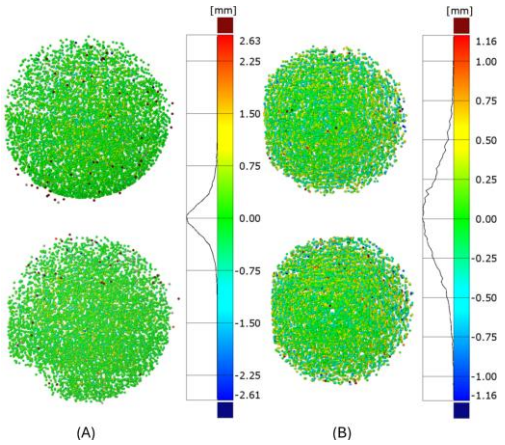

Figure 9. Fitting spheres of (A) temporal and (B) spatiotemporal correlation reconstruction.

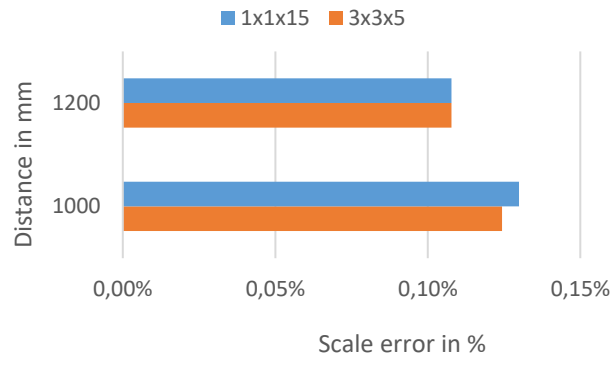

Figure 11. Scale error betwen normalized fitted sphere centres distance from temporal (blue) and spatiotemporal (orange) technique.

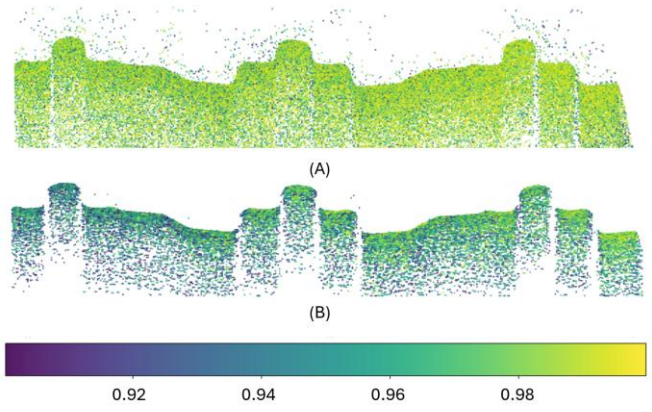

Figure 12. Point cloud reconstruction of pipe-like section from temporal (A) and spatiotemporal (B) correlation technique. The colour of the points represents the correlation factor of each point.

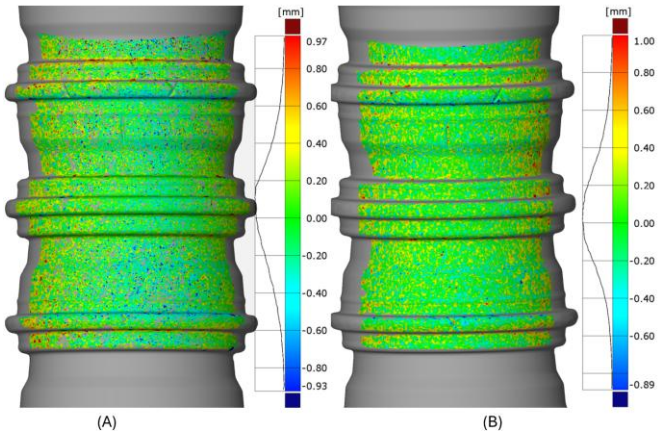

Figure 13. Surface adjustment over reference object from temporal (A) and spatiotemporal (B) correlation technique.

algorithms was virtually identical, with errors converging at approximately 0.11 %. These results confirm that the reduction in data acquisition volume, from 15 images to 5, achieved via the spatiotemporal algorithm, does not compromise the global geometric accuracy of the measurement.

3.4. Surface reconstruction

To validate the applicability of the proposed method to complex, free-form geometries typical of industrial inspection scenarios, a qualitative evaluation was conducted using a pipe-like component. This object features varying surface curvatures and occlusion challenges that surpass the complexity of the planar and spherical artefacts previously analysed. The primary objective of this test was to assess the robustness of the spatiotemporal correlation algorithm in maintaining surface continuity and high correlation reliability under less idealized conditions.

The reconstruction utilizing the purely temporal approach ($1 \times 1 \times 15$), shown in Figure 12 (A), highlights a critical limitation regarding measurement uncertainty. While the method retrieves the general geometry, the point cloud exhibits a significant dispersion of outliers surrounding the actual surface. Notably, the correlation map reveals that many of these erroneous points, located outside the physical object boundary, possess high correlation factors. This phenomenon indicates that, in the absence of spatial constraints, the temporal signature alone may yield false positives, where noise patterns inadvertently maximize the correlation function, thereby introducing ambiguity into the depth estimation.

In contrast, the spatiotemporal reconstruction ($3 \times 3 \times 5$), depicted in Figure 12 (B), demonstrates a substantial improvement in signal integrity. The application of the spatial mask effectively filters out the stochastic noise observed in the temporal model, resulting in a cleaner point cloud with fewer outliers. Crucially, while spatial averaging kernels often risk over smoothing geometric discontinuities, the results indicate that the mask preserves the morphological fidelity of the object. The edges of the pipe and the transitions in curvature remain sharp and well-defined, confirming that the spatiotemporal kernel successfully suppresses correlation noise without compromising the resolution of surface boundaries.

To quantitatively complement these findings, Figure 13 displays the 3D deviation colormaps against a nominal reference model. The temporal approach, Figure 13 (A), exhibits a highly dispersed error distribution, characterized by scattered clusters of positive and negative deviations. This spatial instability is reflected in its wider, flatter error distribution curve, confirming higher dimensional uncertainty.

In contrast, the spatiotemporal reconstruction, Figure 13 (B), shows a significantly more homogeneous error distribution. This quantitative behavior confirms that the spatiotemporal kernel drastically reduces standard deviation and enhances global dimensional precision without losing morphological accuracy.

3.5. Computational effort

In addition to metrological accuracy, the computational performance of the reconstruction algorithms was evaluated to assess their viability for industrial applications where processing time is a critical constraint. Both correlation algorithms were implemented using the PyTorch framework to leverage massive parallelism and GPU acceleration. The performance benchmarks were conducted on a workstation equipped with an NVIDIA GeForce RTX 4070 (8 GB GDDR6) graphics processing unit.

The analysis focused on the total processing time required to reconstruct the measurement volume using input images with a resolution of 4 Megapixels, applied to a grid with a lateral step of $sXY = 1$ mm and a depth step of $sZ = 0.1$ mm. The baseline temporal correlation method, which relies on a sequence of 15 images, required an average processing time of 238 seconds. This duration is largely attributed to the massive data throughput and memory bandwidth required to process the extended sequence of high-resolution, 4 MP frames for every voxel in the dense measurement volume.

In contrast, the optimized spatiotemporal method, which utilizes a reduced sequence of only 5 images combined with a spatial kernel, achieved a significantly reduced processing time of 17 seconds. The decrease in the number of processed frames results in a 14-fold increase in processing speed (approximately 93 % reduction in computational effort). This dramatic efficiency gain, combined with the maintenance of metrological integrity, highlights the spatiotemporal method as a superior candidate for time-sensitive inspection tasks.

4. CONCLUSION AND PROSPECT WORKS

This paper presented an innovative active stereo vision approach that integrates inverse triangulation with spatiotemporal correlation, using a variable pseudorandom pattern projector. Unlike conventional stereo matching algorithms that operate primarily in the image domain, the

proposed method performs the correspondence search directly in object space, using structured three-dimensional patches.

The primary contribution of this work lies in the optimization and validation of the spatiotemporal correlation volume. Through a rigorous parameter analysis, it was determined that a spatiotemporal kernel of size (3 × 3 × 5) provides the optimal balance between measurement accuracy and data acquisition efficiency. The experimental results demonstrate that this configuration reduces the number of required images from 15 to just 5, representing a 66 % reduction in acquisition time and data storage requirements.

Despite this significant reduction in input data, the proposed method maintains, and in some cases surpasses, the metrological performance of the baseline temporal approach (1 × 1 × 15). The validation process, utilizing calibrated artifacts, revealed that the spatiotemporal method achieves a probing error of 0.30 mm and a scale error below 0.12 %. Furthermore, comparative analysis at extended standoff distances highlighted the superior robustness of the spatiotemporal technique, which successfully mitigated the noise and signal degradation that compromised the temporal method. Qualitative reconstructions of complex geometries, such as pipe-like sections, further confirmed the method's ability to reduce outliers while preserving essential morphological features.

Future research will focus on the application of this system to the underwater inspection of offshore structures within the oil and gas industry. The robustness of the spatiotemporal correlation against the specific challenges of the underwater environment, such as turbidity, scattering, and light absorption, will be investigated. Additionally, we intend to integrate this vision system into the "Remotely Operated Vehicle for Underwater Inspection – VORIS" project to validate its performance in dynamic, real-world operational scenarios.

ACKNOWLEDGEMENT

This work was supported by the project “Remotely Operated Vehicle for Underwater Inspection – VORIS”, funded by MCTI/FINEP/FNDCT (Grant No. 0354/23), and carried out by the Laboratory of Metrology and Automation (LABMETRO), Department of Mechanical Engineering, Federal University of Santa Catarina (UFSC).

REFERENCES

[1] J. Geng, Structured-light 3D surface imaging: a tutorial, Adv Opt Photonics vol. 3 (2011) no. 2, pp. 128–160. DOI: 10.1364/aop.3.000128

[2] C. Reich, R. Ritter, J. Thesing, 3-D shape measurement of complex objects by combining photogrammetry and fringe projection, Optical Engineering vol. 39 (2000) no. 1, pp. 224–231. DOI: 10.1117/1.602356

[3] W. Jang, C. Je, Y. Seo, S. W. Lee, Structured-light stereo: Comparative analysis and integration of structured-light and active stereo for measuring dynamic shape, Opt Lasers Eng. vol. 51 (2013) no. 11, pp. 1255–1264. DOI: 10.1016/j.optlaseng.2013.05.001

[4] D. Khan, M. A. Shirazi, M. Y. Kim, Single shot laser speckle based 3D acquisition system for medical applications, Opt Lasers Eng. vol. 105 (2018), pp. 43–53. DOI: 10.1016/j.optlaseng.2018.01.001

[5] M. Dekiff, P. Berssenbrügge, B. Kemper, C. Denz, D. Dirksen, Three-dimensional data acquisition by digital correlation of projected speckle patterns, Appl Phys B vol. 99 (2010) no. 3, pp. 449–456. DOI: 10.1007/s00340-010-3978-x

[6] S. Heist, P. Lutzke, P. Dietrich, P. Kühmstedt, G. Notni, Experimental comparison of laser speckle projection and array projection for high-speed 3D measurements, Proc. of SPIE 9525, Optical Measurement Systems for Industrial Inspection IX, 22 June 2015, p. 952515. DOI: 10.1117/12.2184672

[7] S. Zhuang, D. Tu, X. Zhang, C. Liu, The influence of active projection speckle patterns on underwater binocular stereo vision 3D imaging, Opt Commun. vol. 528 (2023), 129014. DOI: 10.1016/j.optcom.2022.129014

[8] Z. Song, S. Tang, F. Gu, C. Shi, J. Feng, DOE-based structured-light method for accurate 3D sensing, Opt Lasers Eng. vol. 120 (2019), pp. 21–30. DOI: 10.1016/j.optlaseng.2019.02.009

[9] D. Scharstein, R. Szeliski, R. Zabih, A taxonomy and evaluation of dense two-frame stereo correspondence algorithms, Proc. of the IEEE Workshop on Stereo and Multi-Baseline Vision (SMBV 2001), Kauai, HI, USA, 2001, pp. 131–140. DOI: 10.1109/SMBV.2001.988771

[10] T. Pinto, C. Kohler, A. Albertazzi, Regular mesh measurement of large free form surfaces using stereo vision and fringe projection, Opt Lasers Eng. vol. 50 (2012) no. 7, pp. 910–916. DOI: 10.1016/j.optlaseng.2012.03.003

[11] T. L. F. da Costa Pinto, E. G. Armando Albertazzi Jr, 3D active stereo measurement in a regular mesh with random pattern and laser speckle projection, ABCM Symposium Series in Mechatronics vol. 6, p. 9. Online [Accessed 22 June 2026] https://www.abcm.org.br/upload/files/PI_II_05.pdf

[12] Y. Lu, Y. Zhou, M. Hei, D. Fan, Theoretical and experimental determination of steering mechanism for Risley prism systems, Appl Opt. vol. 52 (2013) no. 7, pp. 1389–1398. DOI: 10.1364/AO.52.001389

[13] L. Di Stefano, S. Mattoccia, F. Tombari, ZNCC-based template matching using bounded partial correlation, Pattern Recognit Lett. vol. 26 (2005) no. 14, pp. 2129–2134. DOI: 10.1016/j.patrec.2005.03.022